Materials Science in Semiconductor Processing 128 (2021) 105734

Contents lists available at ScienceDirect

Materials Science in Semiconductor Processing

journal homepage: http://www.elsevier.com/locate/mssp

Electrical transport properties of thermally stable n-ZnO/AlN/p-Si diode grown using RF sputtering

Chandra Prakash Gupta [a], Amit Kumar Singh [a,*], Praveen K. Jain [b], Shashi Kant Sharma [c], Shilpi Birla [a], Sandeep Sancheti [d]

[a] Department of Electronics and Communication Engineering, Manipal University Jaipur, 303007, Rajasthan, India
[b] Department of Electronics and Communication Engineering, Swami Keshvanand Institute of Technology, Management & Gramothan, Jaipur, 302017, Rajasthan, India
[c] Department of Electronics and Communication Engineering, Indian Institute of Information Technology, Ranchi, Jharkhand, India
[d] SRM Institute of Science and Technology, Chennai, Tamilnadu, 603203, India

ARTICLE INFO

Keywords:
Electrical properties
RF Sputtering
ZnO
Thermal stability

ABSTRACT

The temperature dependent electrical transport properties of n-ZnO/AlN/p-Si heterojunction diode fabricated by RF sputtering system have been investigated over a wide temperature range of 303 K–413 K. The AlN buffer layer in-between ZnO and Si lowers the mismatch in thermal expansion coefficient/lattice constant for improved electrical and structural characteristics. XRD pattern and FESEM confirm the crystalline nature and good quality of ZnO thin film with uniform grain size and crack free structure respectively. As measured from the temperature dependent I–V curve, the apparent barrier height reduces as Ideality factor rises which shows good thermal stability within the temperature range studied here. The mean value of barrier height as well as the Richardson constant have been evaluated. Additionally, by taking into account the Gaussian distribution of inhomogeneous barrier heights, the modified Richardson constant has been estimated.

1. Introduction

Currently, Zinc oxide has drawn a great interest due to its exceptional electronics, optoelectronics, piezoelectronics and mechanical properties [1–4]. ZnO has a high value of excitation binding energy (60 meV) and a wide bandgap (3.37eV) [4]. ZnO nanostructures such as nano-rod (NR), nano-wire (NW), and nano-plates (NP) have been extensively studied in recent years [5–7]. These structures possess unique properties and are used in different applications such as UV detectors, photodetectors, bio-sensors, light emitting diodes, gas sensors and memories etc. [8–11]. Diverse heterojunction nano-devices such as *p*-NiO/n-ZnO [12], n-ZnO/p-Si [13], *p*-$SrCu_2O_2$/n-ZnO [14] have been investigated in the recent past. However, p-Si/n-ZnO heterojunction devices have been found appropriate for consumer applications due to the inexpensiveness of silicon technology. The interface quality of two different bandgap materials significantly affects the performance of semiconductor devices. Introduction of suitable buffer layers can be very helpful in reducing this mismatch at the interface of two materials with different bandgaps and can enhance the device performance significantly [15]. I–V measurements were done to determine the carrier transport mechanism in *p*-ZnO/n-Si Heterojunction and the turn-on voltage at 21 °C has been reported to be ~1.35 V [16]. Current-voltage characteristics of LiNiO/MgZnO/ZnO diode was examined and the MgZnO layer was observed to reduce the leakage current [17]. Current-voltage characteristics i-ZnO/n-ZnO/n-Si structure was investigated and activation energy and the Richardson constant have been reported [18]. Current-voltage characteristics n-ZnO/p-GaN heterojunction ultraviolet-blue LED fabricated using metal-organic chemical vapor deposition has been reported [19]. In this paper, the temperature dependent V–I curve of RF sputtered deposited n-ZnO/AlN/p-Si heterojunction diodes has been reported. AlN has been used as buffer layer to improve the surface quality between ZnO and silicon. For the temperature range of 303–413 K, the physical parameters of the heterostructure diode namely reverse saturation current, barrier height, ideality factor and Richardson constant have been investigated. In section 2, ZnO thin film preparation process and device characterization has been discussed. Section 3 presents a discussion on the device design and the experimental results followed finally by the conclusion section.

* Corresponding author.
E-mail address: amitkumarsingh89@gmail.com (A.K. Singh).

https://doi.org/10.1016/j.mssp.2021.105734
Received 30 September 2020; Received in revised form 30 December 2020; Accepted 27 January 2021
Available online 13 February 2021

2. Experimental setup

2.1. ZnO thin film growth

In the first step, the standard RCA cleaning method has been used to clean boron doped 2-inch p-type Si (100) substrate for device fabrication. After cleaning of the Si substrate, AlN thin film was grown using the RF sputtering method by the deposition of Al in the presence of N_2 and Ar gas. There after ZnO thin film was also grown. For the measurement of electrical characteristics, Al resistive contacts were developed using RF sputtering method. Various parameters used during the deposition at 300 K have been stated in Table 1.

2.2. Characterization of n-ZnO/AlN/p-Si diode

The surface morphology as well as the crystalline structure of the ZnO thin film has been characterized using XRD (X-ray diffractometer) - (XDMAX, PC-20, Rigaku) and SEM (scanning electron microscope) - (Nova Nano FE-SEM 450) respectively. Measurement of current-voltage characteristics of the n-ZnO/AlN/p-Si heterojunction diode was performed using Keithley electrometer with probe station (B1500A-Semiconductor Parameter Analyzer).

3. Results and discussion

The schematic of the fabricated n-ZnO/AlN/p-Si heterostructure diode is shown in Fig. 1. The XRD diffraction pattern of ZnO as shown in Fig. 2(a) confirms the dominating c-axis (002) orientation in the hexagonal wurtzite structure. Fig. 2(b) depicts the SEM representation of ZnO thin film which reveals good quality film with uniform grain size and crack free structure.

The experimentally observed I–V characteristics of n-ZnO/AlN/p-Si heterostructure diode with the variation of temperature starting from 303 K to 413 K is presented in Fig. 3, which confirms the rectifying nature of the p-n junction diode. Further, the turn-on voltage was observed at about 0.82 V at room temperature. For the analysis of diode physical parameters, the standard thermionic emission model was utilized for the fabricated diode. The current in terms of voltage for standard thermionic emission is expressed as [13].

$$I = I_0\left[\exp\left(\frac{V}{\eta V_T}\right) - 1\right] \tag{1}$$

where $V_T = \frac{kT}{q}$ thermal voltage, I_0 = reverse saturation current, V = voltage applied at bias and η being the ideality factor given as [20].

$$\eta = \left[\frac{1}{V_T}\frac{dV}{d\ln(I)}\right] \tag{2}$$

The effective barrier height (zero bias) can be given as [21].

Table 1
Deposition Parameters for ZnO and AlN thin films deposited by RF sputtering at 300 K.

Parameters	AlN thin film	ZnO thin film	Al Contact (Top & Bottom)
Thickness (nm)	30	250	100
Ambient Gas (Sccm)	Ar & N_2 (15)	Ar (20)	Ar (15)
Deposition Power (watt)	100	100	100
Background Pressure (mbar)	$\sim 1 \times 10^{-6}$	$\sim 1 \times 10^{-6}$	$\sim 1 \times 10^{-6}$
Deposition Pressure (mbar)	$\sim 4 \times 10^{-3}$	$\sim 1 \times 10^{-3}$	$\sim 1 \times 10^{-3}$
Deposition Rate (per second) in Å	0.3–0.8	0.5–1.1	0.3–0.6
Deposition Time (min)	~ 10	~55	~ 50

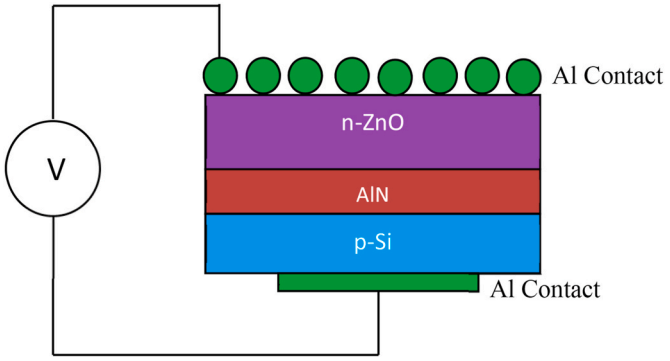

Fig. 1. Schematic diagram of designed n-ZnO/AlN/p-Si heterostructure diode.

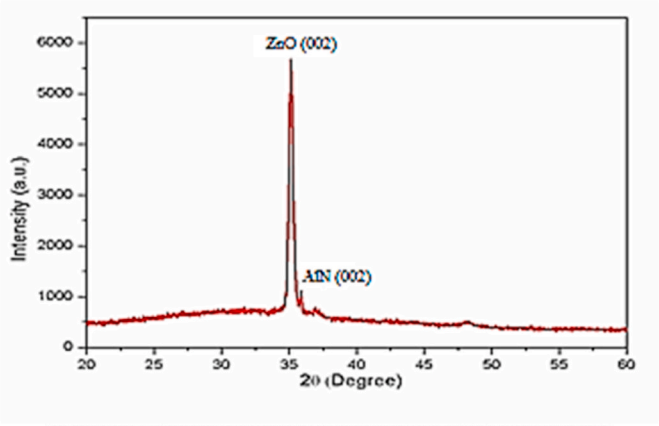

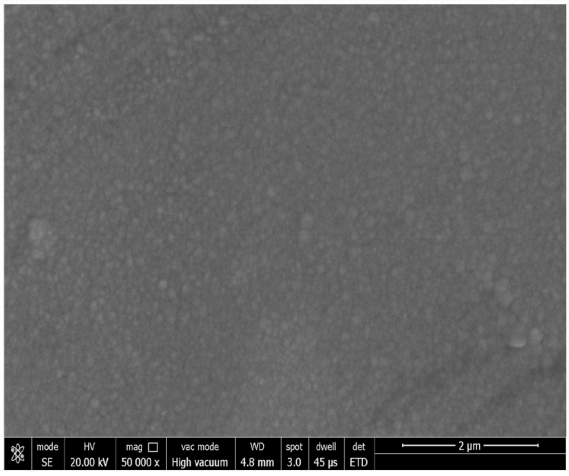

Fig. 2. (a) XRD pattern, 2(b) SEM image of the deposited ZnO thin film at 300 K.

$$\varphi_{B,eff} = V_T ln\left(\frac{AA^*T^2}{I_o}\right) \tag{3}$$

where, A is contact area i.e. $\sim 0.785 \times 10^{-2}$ cm^2 (for this study), A^* is the effective Richardson constant ($A^* = 32\text{Acm}^{-2}\text{k}^{-2}$; for $m_e^* = 0.27m_0$) . The proportionate relationship of reverse current and temperature as indicated by eq. (3) refers to the high dependency of reverse current on temperature. This is also confirmed by the experimentally observed I–V-T curve shown in Fig. 3. Slight non-saturation in current with applied bias has also been observed in I–V-T curve. This non-saturation arises due to the spatial inhomogeneity of barrier height in reverse bias and higher values of the SDOS (surface density of states) close to the

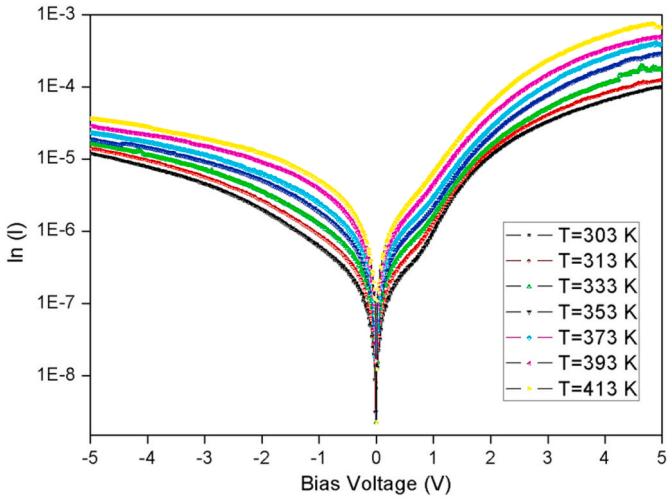

Fig. 3. I–V Characteristics of n-ZnO/AlN/p-Si heterojunction diode with variation of temperature from 303 K to 413 K.

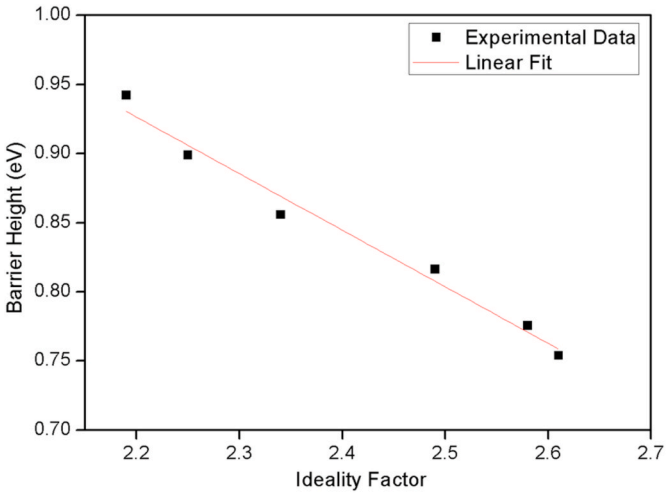

Fig. 4. Variation of Barrier height with ideality factor over the temperature 313 K–413 K.

conduction band and resistance of the device in forward bias voltage [22,23].

The values of I_o, $\varphi_{B,eff}$ and η have been estimated from the I–V-T characteristics curve for the temperature range from 303 K to 393 K are shown in Table 2. These results affirm the better thermal stability of n-ZnO/AlN/p-Si diode. It has been seen that I_0 and $\varphi_{B,eff}$ increase with temperature, on the other hand η decreases with temperature rise. The calculated value of $\eta > 1$ for the entire range of temperature indicates the inhomogeneity at n-ZnO/AlN/p-Si interface. It also depicts that the possible current transport mechanisms of current conduction are thermionic emission, diffusion, space charge region recombination and tunneling for fabricated n-ZnO/AlN/p-Si heterostructure diode. The change in the value of barrier height with ideality factor is linear as presented in Fig. 4 which attributes to the irregularity of barrier and inhomogeneities of barrier height.

For the calculation of Richardson constant (A*), eq. (3) can be reorganized as a linear relation between $ln(I_0/T^2)$ and $\frac{1}{V_T}$ [21,22].

$$\ln\left(\frac{I_0}{T^2}\right) = \ln(AA^*) - \frac{\varnothing_{B0}}{V_T} \tag{4}$$

Moreover, the Richardson constant and barrier height was evaluated from the intercept and slope of the linear curve between $ln(I_0/T^2)$ and $\frac{1}{V_T}$ respectively. The measured values of Richardson constant and barrier height are 2.709×10^{-13} Acm^{-2} K^{-2} and 125 meV respectively. This considerable difference in the value of experimental Richardson constant value from its theoretical value i.e. 32 $Acm^{-2}K^{-2}$ is due to inhomogeneities of barrier height at the interface.

Gaussian distribution function with variance of σ_0^2 and mean barrier height has been utilized to overcome the drawback of inhomogeneities at the contact. The Barrier height and ideality factor relationship with Gaussian distribution can be illustrated as [21,22].

Table 2
Temperature dependent reverse saturation current (I_o), ideality factor (η) and barrier height (φ_B) for n-ZnO/AlN/p-Si diode.

Temperature (K)	Barrier Height φ_B (eV)	Reverse Saturation Current I_o (A)	Ideality Factor η
303	0.753883	6.66×10^{-9}	2.61
313	0.775578	8.00×10^{-9}	2.58
333	0.816321	1.23×10^{-8}	2.49
353	0.855859	1.89×10^{-8}	2.34
373	0.898970	2.49×10^{-8}	2.25
393	0.942187	3.31×10^{-8}	2.19

$$\varnothing_{B,\,eff}(T) = \varnothing_{B0,m}(T=0) - \frac{\sigma_0^2}{2V_T} \tag{5}$$

$$\left(\frac{1}{\eta(T)} - 1\right) = \rho_1 - \frac{\rho_2}{2V_T} \tag{6}$$

Where $\eta(T)$ is ideality factor at the given temperature, $\varnothing_{B,m}(V) = \varnothing_{B0,m} + \rho_1 V$ is the mean barrier height at the given bias voltage, ρ_1 and ρ_2 are voltage coefficients, $\sigma^2(V) = \sigma_0^2 + \rho_2 V$ is the standard deviation at the given bias voltage. The linear fit variation of barrier height with $\frac{1}{2V_T}$ is shown in Fig. 6. The intercept and slope of linear fit curve gives the values of $\varnothing_{B,0m}(T=0) = 1.56$ eV and $\sigma_0 = 0.2056$ V, respectively. Further, linear fit curve of η^{-1}-1 Vs $\frac{1}{2V_T}$ as shown in Fig. 7 gives $\rho_1 = 0.2817\ V$ and $\rho_2 = 0.0177\ V$. If the inhomogeneities of barrier height is considered, then the Richardson constant can be modified as [21].

$$\ln\left(\frac{I_0}{T^2}\right) - \left(\frac{\sigma_0^2}{2(V_T)^2}\right) = \ln(AA^*) - \frac{\varnothing_{B0,m}(T=0)}{V_T} \tag{7}$$

The linear fitting curve of $\ln(I_0/T^2)$-$\sigma_0^2/2(V_T)^2$ and $\frac{1}{V_T}$ as shown in Fig. 8 provides the value of $\varnothing_{B,m}(V)$ and A*. The calculated value of $\varnothing_{B,m}(V)$ and A* are 1.56 eV and 39.93 $Acm^{-2}K^{-2}$ respectively.

The modified Richardson constant obtained is very near to the

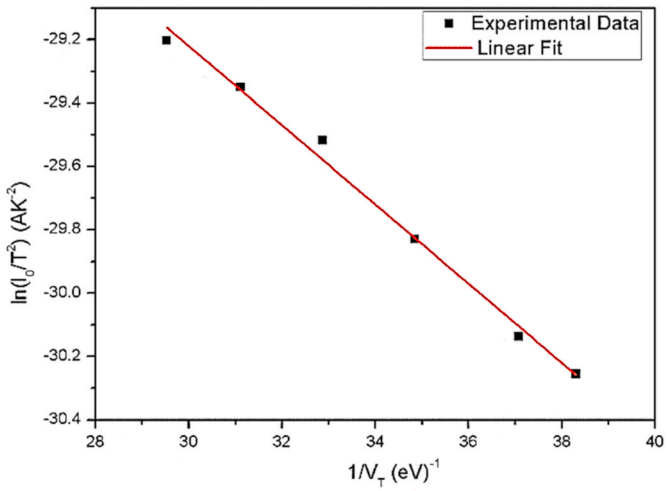

Fig. 5. The plot between $ln(I_0/T^2)$ and $\frac{1}{V_T}$ for the calculation of A^* and φ_{Bo}

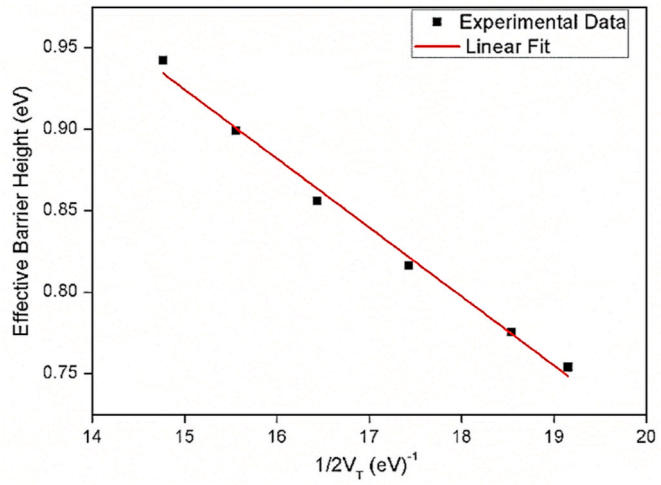

Fig. 6. The plot between effective barrier height and $\frac{1}{2V_T}$

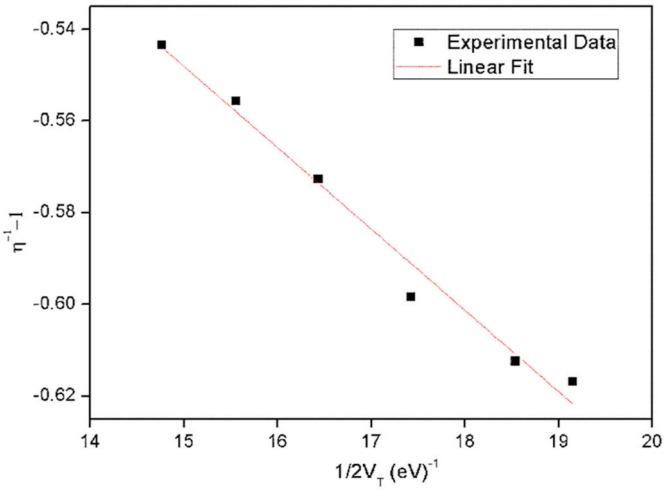

Fig. 7. The plot between η^{-1}-1 and $\frac{1}{2V_T}$ for different parameters calculation.

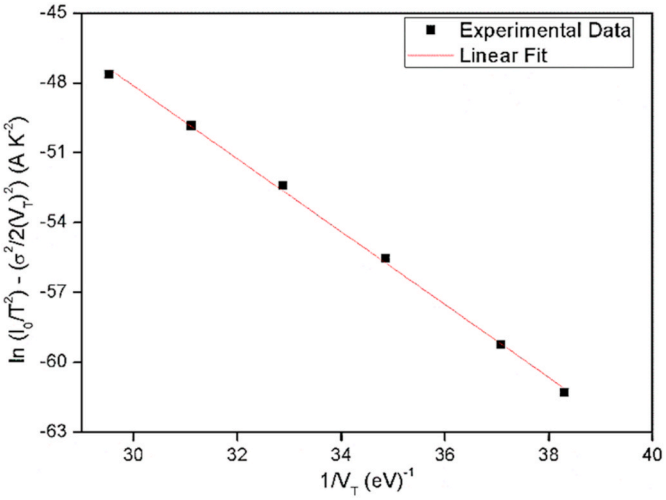

Fig. 8. The plot between $\ln(I_0/T^2)$-$\sigma_0^2/2(V_T)^2$ and $\frac{1}{V_T}$ to calculate modified Richardson constant.

theoretical value of Richardson constant i.e. 32 $Acm^{-2}K^{-2}$, which is due to consideration of inhomogeneities phenomenon of barrier height. This value of the modified Richardson constant obtained is better than the values reported by several other works [21,24,25] reported in literature recently.

The value of activation energy in n-ZnO/p-Si heterojunction fabricated using ultrasonic spray has been reported to be 140 meV [26]. In n-ZnO/p-Si heterojunctions grown using pulsed laser deposition technique, activation energy of 360 meV has been observed [27]. The barrier height can be supposed to be the activation energy generally [28–30]. In the present work as per Fig. 5, Barrier height of 125 meV has been obtained.

Fig. 9 shows the band diagram of n-ZnO/p-Si heterostructure diode and Fig. 10 shows the Band diagram of n-ZnO/AlN/p-Si heterostructure diode. The energy bandgaps of ZnO, Si and AlN have been used as 3.37 [31,32], 1.12, and 6.2 eV [33] respectively. The electron affinities of ZnO, Si, and AlN have used as 4.5, 4.05 [34] and 0.6 eV [35] respectively. Bandgap narrowing and low field carrier mobility physical models have been used in the simulations. For the current simulations of bandstructure, Si and ZnO layer thickness is taken to be 250 nm while the AlN thickness is 30 nm. As observed from the band diagram of Si/AlN/ZnO heterostructure, there is a smaller valence band offset and a larger conduction band offset in between AlN and ZnO layers as compared to the band offsets in Si/ZnO heterostructure. Due to the typical band offsets, the AlN layer acts as a charge carrier blocking layer.

4. Conclusion

A systematic study of electric transport characteristics of n-ZnO/AlN/p-Si heterostructure diode successfully fabricated using sputtering technique has been performed. The junctions show the rectifying nature and turn-on voltage of the diode is about 0.82 V at room temperature. Barrier height decreases as Ideality factor increases depicting good thermal stability within the temperature range considered here. The relationship between Ideality factor and the barrier height was observed to be linear. The calculated modified Richardson constant is about 39.93 Acm^2K^{-2} by considering the Gaussian distribution which is very near to the theoretical value of Richardson constant i.e. 32 Acm^2K^{-2}.

CRediT authorship contribution statement

Chandra Prakash Gupta: Conceptualization, Conception and design of study, Funding acquisition, Acquisition of data, Formal

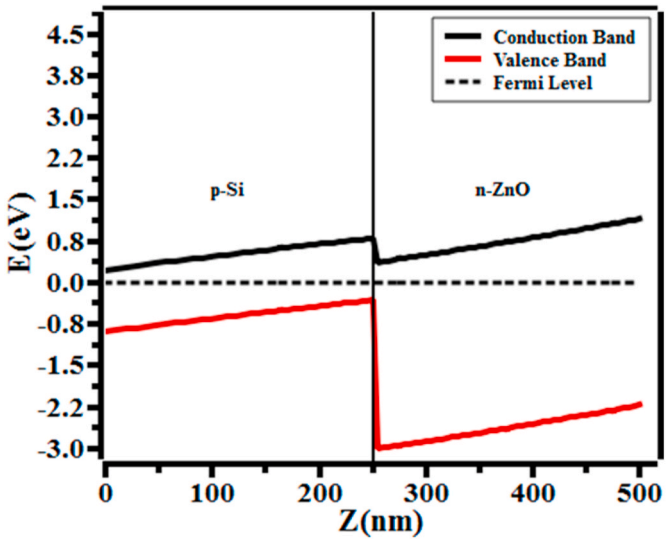

Fig. 9. Band diagram of n-ZnO/p-Si heterostructure diode.

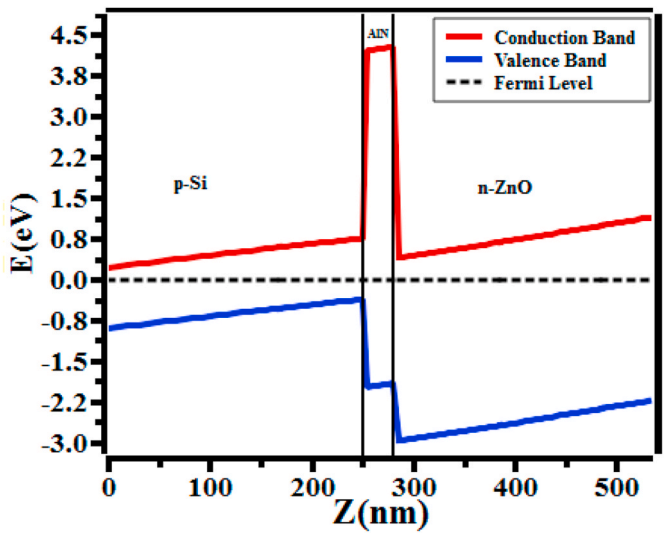

Fig. 10. Band diagram of n-ZnO/AlN/p-Si heterostructure diode.

analysis, Analysis and/or interpretation of data, Writing - original draftWriting – original draft, Drafting the manuscript, Revising the manuscript critically for important intellectual content, Approval of the version of the manuscript to be published. **Amit Kumar Singh:** Writing - original draftWriting – original draft, Drafting the manuscript, Revising the manuscript critically for important intellectual content, Approval of the version of the manuscript to be published. **Praveen K. Jain:** Conceptualization, Conception and design of study, Formal analysis, Analysis and/or interpretation of data, Writing - original draftWriting – original draft, Drafting the manuscript, Revising the manuscript critically for important intellectual content, Approval of the version of the manuscript to be published. **Shashi Kant Sharma:** Conceptualization, Conception and design of study, Funding acquisition, Acquisition of data, Formal analysis, Analysis and/or interpretation of data, Writing - original draftWriting – original draft, Drafting the manuscript, Revising the manuscript critically for important intellectual content, Approval of the version of the manuscript to be published. **Shilpi Birla:** Conceptualization, Conception and design of study, Funding acquisition, Acquisition of data, Formal analysis, Analysis and/or interpretation of data, Writing - original draftWriting – original draft, Drafting the manuscript, Revising the manuscript critically for important intellectual content, Approval of the version of the manuscript to be published. **Sandeep Sancheti:** Conceptualization, Conception and design of study, Formal analysis, Analysis and/or interpretation of data, Writing - original draftWriting – original draft, Drafting the manuscript, Revising the manuscript critically for important intellectual content, Approval of the version of the manuscript to be published.

Declaration of competing interest

The authors declare that they have no known competing financial interests or personal relationships that could have appeared to influence the work reported in this paper.

Acknowledgement

Authors acknowledge Semiconductor Device Fabrication Laboratory, Manipal University Jaipur and the Materials Research Centre, MNIT Jaipur for extending their device fabrication and characterization facilities. Authors are also thankful to Manipal University Jaipur for the financial aid through the Seed Grant Project MUJ/REGR/1435/08.

References

[1] V. Subramanian, T. Bakhishev, D. Redinger, S.K. Volkman, Solution-processed zinc oxide transistors for low-cost electronics applications, IEEE/OSA J. Disp. Technol. 5 (2009) 525–530, https://doi.org/10.1109/JDT.2009.2029124.
[2] S. Sharma, S. Vyas, C. Periasamy, P. Chakrabarti, Structural and optical characterization of ZnO thin films for optoelectronic device applications by RF sputtering technique, Superlattice. Microst. 75 (2014) 378–389, https://doi.org/10.1016/j.spmi.2014.07.032.
[3] K. Tao, H. Yi, L. Tang, J. Wu, P. Wang, N. Wang, L. Hu, Y. Fu, J. Miao, H. Chang, Piezoelectric ZnO thin films for 2DOF MEMS vibrational energy harvesting, Surf. Coating. Technol. 359 (2019) 289–295, https://doi.org/10.1016/j.surfcoat.2018.11.102.
[4] S.K.M. Bakhori, S. Mahmud, D. Mohamad, S.M. Masudi, A. Seeni, Surface morphological and mechanical properties of zinc oxide eugenol using different types of ZnO nanopowder, Mater. Sci. Eng. C 100 (2019) 645–654, https://doi.org/10.1016/j.msec.2019.03.034.
[5] M. Yang, S. Zhang, F. Qu, S. Gong, C. Wang, L. Qiu, M. Yang, W. Cheng, High performance acetone sensor based on ZnO nanorods modified by Au nanoparticles, J. Alloys Compd. 797 (2019) 246–252, https://doi.org/10.1016/j.jallcom.2019.05.101.
[6] N.K. Park, G.B. Han, J.D. Lee, S.O. Ryu, T.J. Lee, W.C. Chang, C.H. Chang, The growth of ZnO nano-wire by a thermal evaporation method with very small amount of oxygen, Curr. Appl. Phys. 6 (2006) 176–181, https://doi.org/10.1016/j.cap.2006.01.034.
[7] C.P. Gupta, S.K. Sharma, B. Bhowmik, K.T. Sampath, C. Periasamy, S. Sancheti, Development of highly sensitive and selective ethanol sensors based on RF sputtered ZnO nanoplates, J. Electron. Mater. 48 (2019) 3686–3691, https://doi.org/10.1007/s11664-019-07127-4.
[8] A. Kolodziejczak-Radzimska, T. Jesionowski, Zinc oxide-from synthesis to application: a review, Materials 7 (2014) 2833–2881, https://doi.org/10.3390/ma7042833.
[9] P.K. Jain, M. Salim, U. Chand, C. Periasamy, Switching characteristics in TiO2/ZnO double layer resistive switching memory device, Mater. Res. Express 4 (2017), 065901, https://doi.org/10.1088/2053-1591/aa731e.
[10] R. Singh, P. Sharma, A. Khan, V. Garg, V. Awasthi, A. Kranti, S. Mukherjee, Investigation of barrier inhomogeneities and interface state density in Au/MgZnO : Ga Schottky contact, J. Phys. D Appl. Phys. 49 (n.d.) 445303. https://doi.org/10.1088/0022-3727/49/44/445303.
[11] R. Bhardwaj, P. Sharma, R. Singh, S. Mukherjee, Sb-Doped p-MgZnO/n-Si heterojunction UV photodetector fabricated by dual ion beam sputtering, IEEE Photon. Technol. Lett. 29 (2017) 1215–1218, https://doi.org/10.1109/LPT.2017.2713701.
[12] H. Ohta, M. Kamiya, T. Kamiya, M. Hirano, H. Hosono, UV-detector based on pn-heterojunction diode composed of transparent oxide semiconductors, p-NiO/n-ZnO, Thin Solid Films 445 (2003) 317–321, https://doi.org/10.1016/S0040-6090(03)01178-7.
[13] S. Chirakkara, S.B. Krupanidhi, Study of n-ZnO/p-Si (100) thin fi lm heterojunctions by pulsed laser deposition without buffer layer, Thin Solid Films 520 (2012) 5894–5899, https://doi.org/10.1016/j.tsf.2012.05.003.
[14] H. Ohta, K.I. Kawamura, M. Orita, M. Hirano, N. Sarukura, H. Hosono, Current injection emission from a transparent p-n junction composed of p-SrCu2O2/n-ZnO, Appl. Phys. Lett. 77 (2000) 475–477, https://doi.org/10.1063/1.127015.
[15] B. Roul, R. Pant, S. Chirakkara, G. Chandan, K.K. Nanda, S.B. Krupanidhi, Enhanced UV photodetector response of ZnO/Si with AlN buffer layer, IEEE Trans. Electron. Dev. 64 (2017) 4161–4166, https://doi.org/10.1109/TED.2017.2741971.
[16] Z. Shi, D. Wu, T. Xu, Y. Zhang, B. Zhang, Y. Tian, X. Li, G. Du, Improved electrical transport and electroluminescence properties of p-ZnO/n-Si heterojunction via introduction of patterned SiO2 intermediate layer, J. Phys. Chem. C (2016), https://doi.org/10.1021/acs.jpcc.5b10689.
[17] T. Dutta, P. Gupta, A. Gupta, J. Narayan, Effect of Li doping in NiO thin films on its transparent and conducting properties and its application in heteroepitaxial p-n junctions, J. Appl. Phys. (2010), https://doi.org/10.1063/1.3499276.
[18] S. Ylmaz, E. Bacaksz, I. Polat, Y. Atasoy, Fabrication and structural, electrical characterization of i-ZnO/n-ZnO nanorod homojunctions, Curr. Appl. Phys. (2012), https://doi.org/10.1016/j.cap.2012.03.021.
[19] Z. Shi, Y. Zhang, J. Zhang, H. Wang, B. Wu, X. Cai, X. Cui, X. Dong, H. Liang, B. Zhang, G. Du, High-performance ultraviolet-blue light-emitting diodes based on an n-ZnO nanowall networks/p-GaN heterojunction, Appl. Phys. Lett. (2013), https://doi.org/10.1063/1.4813538.
[20] C. Periasamy, P. Chakrabarti, Effect of temperature on the electrical characteristics of nanostructured n-ZnO/p-Si heterojunction diode, Sci. Adv. Mater. 5 (2013) 1384–1391, https://doi.org/10.1166/sam.2013.1580.
[21] D. Somvanshi, S. Jit, Mean barrier height and richardson constant for Pd/ZnO Thin film-based Schottky Diodes grown on n-Si substrates by thermal evaporation method, IEEE Electron. Device Lett. 34 (2013) 1238–1240, https://doi.org/10.1109/LED.2013.2278738.
[22] D.E. Yildiz, Ş. Altindal, H. Kanbur, Gaussian distribution of inhomogeneous barrier height in Al/SiO 2/p-Si Schottky diodes, J. Appl. Phys. 103 (2008) 124502, https://doi.org/10.1063/1.2936963.
[23] H.H. Güllü, Investigation of electrical properties of In/ZnIn2Te4/n-Si/Ag diode, Bull. Mater. Sci. 42 (2019) 89, https://doi.org/10.1007/s12034-019-1770-z.
[24] S. Ranwa, P. Kumar Kulriya, V. Dixit, M. Kumar, Temperature dependent electrical transport studies of self-aligned ZnO nanorods/Si heterostructures deposited by sputtering, J. Appl. Phys. 115 (2014), https://doi.org/10.1063/1.4883961, 0–6.

[25] W. Mtangi, F.D. Auret, C. Nyamhere, P.J. Janse van Rensburg, M.D.A. Chawanda, Analysis of temperature dependent I - V measurements on Pd/ZnO Schottky barrier diodes and the determination of the Richardson constant, Phys. B Condens. Matter 404 (2009) 1092–1096, https://doi.org/10.1016/j.physb.2008.11.022.

[26] N. Zebbar, Y. Kheireddine, K. Mokeddem, A. Hafdallah, M. Kechouane, M.S. Aida, Structural, optical and electrical properties of n-ZnO/p-Si heterojunction prepared by ultrasonic spray, Mater. Sci. Semicond. Process. (2011), https://doi.org/10.1016/j.mssp.2011.03.001.

[27] S. Chand, R. Kumar, Electrical characterization of Ni/n-ZnO/p-Si/Al heterostructure fabricated by pulsed laser deposition technique, J. Alloys Compd. (2014), https://doi.org/10.1016/j.jallcom.2014.06.042.

[28] F. Schipani, C.M. Aldao, M.A. Ponce, Schottky barriers measurements through Arrhenius plots in gas sensors based on semiconductor films, AIP Adv. (2012), https://doi.org/10.1063/1.4746417.

[29] I.D. Kim, A. Rothschild, T. Hyodo, H.L. Tuller, Microsphere templating as means of enhancing surface activity and gas sensitivity of CaCu 3Ti 4O 12 thin films, Nano Lett. (2006), https://doi.org/10.1021/nl051965p.

[30] R. Ionescu, C. Moise, A. Vancu, Are modulations of the Schottky surface barrier the only explanation for the gas-sensing effects in sintered SnO2? Appl. Surf. Sci. (1995) https://doi.org/10.1016/0169-4332(94)00544-3.

[31] A. Mang, K. Reimann, S. Rübenacke, Band gaps, crystal-field splitting, spin-orbit coupling, and exciton binding energies in ZnO under hydrostatic pressure, Solid State Commun. (1995), https://doi.org/10.1016/0038-1098(95)00054-2.

[32] F. Benharrats, K. Zitouni, A. Kadri, B. Gil, Determination of piezoelectric and spontaneous polarization fields in Cdx Zn1 - x O/ZnO quantum wells grown along the polar ⟨ 0001 ⟩ direction, Superlattice. Microst. (2010), https://doi.org/10.1016/j.spmi.2010.01.007.

[33] H. Yamashita, K. Fukui, S. Misawa, S. Yoshida, Optical properties of AlN epitaxial thin films in the vacuum ultraviolet region, J. Appl. Phys. (1979), https://doi.org/10.1063/1.326007.

[34] B.G. Budaguan, A.A. Aivazov, A.A. Sherchenkov, A.V. Biriukov, V. D. Chernomordic, J.W. Metselaar, Properties of a-Si:H/c-Si heterostructures prepared by 55 kHz PECVD for solar cell application, in: Mater. Res. Soc. Symp. - Proc, 1998, https://doi.org/10.1557/proc-485-303.

[35] M.S.M. Levinshtein, S. Rumyantsev, Properties of Advanced Semiconductor Materials: GaN, AlN, InN, SiC, SiGe,BN, 1994.